ELSEVIER

International Journal of Heat and Fluid Flow 19 (1998) 201–207

International Journal of HEAT AND FLUID FLOW

Effects of micro-mixing in gas-phase turbulent jets

H.A. Wouters *, P.A. Nooren, T.W.J. Peeters, D. Roekaerts

Heat Transfer Section, Delft University of Technology, Lorentzweg 1, 2628 CJ Delft, The Netherlands

Received 8 August 1997; accepted 25 October 1997

Abstract

Scalar mixing in turbulent jets is modeled using a hybrid Monte Carlo PDF method which solves for the joint velocity-scalar PDF. Molecular scalar mixing is modeled by: Interaction by Exchange with the Mean, Coalescence/Dispersion (C/D), Binomial Langevin and Mapping Closure models. The concentration field statistics adopt a self-similar solution along rays emerging from the jets virtual origin. Predicted PDF's of the normalized concentration are compared to measurements. All mixing models yield good agreement with the measurements at all radial and axial positions. The C/D model gives the best results close to the centerline but at the edge of the jet, the model predicts unrealistic PDF shapes.

Keywords: PDF methods; Monte Carlo method; Mcro-missing; Modeling

1. Introduction

In recent years, the Monte Carlo PDF approach has found many applications in the modeling of turbulent reacting flows. The main benefit of the method lies in the ability to treat the mean chemical source terms exactly without a-priori assumptions on joint multi-scalar statistics (Pope, 1990). In the transport equations for the scalar PDF, the effects of molecular diffusion or 'micro-mixing' occur in unclosed form (Pope, 1985). The objective of this study is to assess the performance of several well-known micro-mixing models in an inert turbulent flow where scalar mixing is representative for the situation in jet diffusion flames.

The configuration studied here is gas-phase mixing in equal-density free turbulent jets. For these flows, concentration measurements were reported by Dowling and Dimotakis (1990). It was found that, along rays emerging from the jets virtual origin, the concentration field statistics adopt a self-similar solution. Comparing results of the self-similar scaled concentration, the scalar PDF's are governed only by the mixing model and the specific flow model is not important.

Simulations are performed with a hybrid Monte Carlo method (Correa and Pope, 1992) which solves for the joint PDF of velocities and scalars. The micro-mixing models considered in this study are: Interaction by Exchange with the Mean, Coalescence/Dispersion, Binomial Langevin and Mapping Closure models. First, predictions of concentration mean and variances are presented to show that the predicted fields are self-similar. Second, PDF's of the normalized concentration are compared with experimental data and with assumed-shape β-function PDF's.

2. Monte Carlo PDF model

2.1. PDF transport equation

In the PDF formulation used here, the transport equation for the one-point joint velocity-scalar PDF is solved. Starting from the transport equations for velocity and composition, the PDF transport equation is derived (Pope, 1985). In this equation, the effects of turbulent convection and chemical reaction occur in closed form. The unclosed terms describe the effects of the fluctuating pressure gradient and molecular diffusion. The evolution in velocity space is modeled by the Simplified Langevin model of Haworth and Pope (1986). Here, we focus on the effects of molecular mixing. Under the influence of micro-mixing, omitting the velocity terms and the effects of convection and reaction, the evolution of the joint velocity-scalar PDF $f_{U\phi}(\boldsymbol{V}, \psi; \boldsymbol{x}, t)$ reads

$$\frac{\partial}{\partial t} f_{U\phi} = -\frac{\partial^2}{\partial \psi_\alpha \partial \psi_\beta}\left[\mathbb{D}\left\langle \frac{\partial \phi'_\alpha}{\partial x_i}\frac{\partial \phi'_\beta}{\partial x_i}\middle| \boldsymbol{U} = \boldsymbol{V}, \phi = \psi\right\rangle f_{U\phi}\right]$$

in which $\mathbb{D}$ is the molecular diffusion coefficient and ϕ'_α, the Reynolds fluctuation of scalar ϕ_α. The expression $\langle\cdot|\cdot\rangle$ denotes the mean value conditional on the velocity and scalar values. Because the statistics of scalar gradients cannot be expressed in terms of the one-point joint velocity-scalar distribution, the conditional average is unclosed and has to be modeled. The effects of this term on the scalar distribution and modeling of this term are described below.

2.2. Monte Carlo solution method

In the Monte Carlo solution method, the PDF is represented by a large ensemble of notional particles with properties like position, velocity and scalar values. The particle properties

* Corresponding author. E-mail: huib@wt.tn.tudelft.nl.

0142-727X/98/$19.00
PII: S0142-727X(97)10025-X

evolve according to particle models such that the evolution of the statistics of the particle ensemble corresponds to the modeled PDF evolution. In our hybrid Monte Carlo solver (Correa and Pope, 1992), the mean fields of velocity, pressure, turbulent kinetic energy and turbulent dissipation are computed externally by a standard finite volume method (FVM) in which turbulence is modeled by a standard k–ϵ model.

2.3. Micro-mixing models

In this study, four models for scalar micro-mixing are considered: the Interaction by Exchange with the Mean, Coalescence/Dispersion, Mapping Closure and Binomial Langevin models. The models satisfy three basic requirements for mixing models. First, the mean value is conserved in the mixing process. Second, the scalar variance decays according to a prescribed decay rate ω_ϕ. This decay rate is modeled by $\omega_\phi = C_\phi\omega = C_\phi\epsilon/k$. The mechanical-to-scalar time-scale ratio C_ϕ is known to vary between 0.5 and 4 for inert scalar mixing (Warhaft and Lumley, 1978) but here it takes the standard value 2. A third property of scalar mixing is the fact that scalar values stay within the physically allowed domain (e.g. mixture fraction is bounded between zero and unity). Even though all models yield the same evolution for the scalar mean and variance, the evolution of the higher moments, and thus the PDF shape, may differ significantly between different models. The mixing models used in this study are described briefly. For a more detailed description of the models see the references given below.

2.3.1. Interaction by exchange with the mean

The Interaction by Exchange with the Mean (IEM) model, also known as the Linear Mean Squares Estimation (LMSE) model (Dopazo, 1975), is defined as a deterministic relaxation of all scalar values to the local mean. The scalar variance decays but the shape of the scalar PDF is conserved in the mixing process.

2.3.2. Coalescence/dispersion

Coalescence/Dispersion (C/D) models are most easily defined in terms of a particle model. Mixing takes place in randomly selected particle pairs that mix, with a certain probability, to the mean value of this pair before mixing (Curl, 1963). Here, a version of the model is used in which the degree of mixing in a particle pair is selected randomly from a uniform distribution (Janicka et al., 1979). Because the configuration is axisymmetrical, not all Monte Carlo particles have equal weights (Haworth and El Tahry, 1990) and a modified expression for the mixing probability has to be used (Nooren et al., 1997).

2.3.3. Mapping closure

The Mapping Closure mode (MCM) is defined as a mapping of the scalar field to a Gaussian reference field (Chen et al., 1989). In the formulation used here, the reference field is stationary and the mapping function evolves in time. The model and its implementation are described by Pope (1991). In pure mixing, an arbitrary initial PDF evolves towards a Gaussian distribution and the mapping function becomes linear.

2.3.4. Binomial Langevin

In the Binomial Langevin (BL) model, the decay of scalar variance is modeled by a linear relaxation to the local mean and the effects of turbulent dispersion are modeled by a stochastic process (Valiño and Dopazo, 1991). The stochastic increments are drawn from a normalized binomial distribution. As a result the stochastic term is bounded. The parameters of the binomial distribution are chosen such that the minimal and maximal values of the increment cannot drive the scalar particles outside the physically allowed domain. Here a modified version of the model is used (see Appendix A).

2.4. Model evaluation

DNS of inert scalar mixing in isotropic homogeneous turbulence (Eswaran and Pope, 1988) showed that the scalar PDF evolves towards a Gaussian distribution. This asymptotic behavior for mixing in homogeneous turbulence is often used to assess mixing model performance. The IEM model predicts the correct evolution of first and second moments but the PDF shape is conserved. C/D models predict an evolution of the scalar PDF towards a bell-shaped function but the normalized even higher moments approach infinity. This means that the limiting PDF is not Gaussian and that the tails of the PDF are overpredicted. MCM and BL models predict the correct PDF evolution. Not only is the asymptotic PDF Gaussian but the PDF agrees well with the DNS data at intermediate times also.

A well known testcase for mixing of reacting scalars is the partially stirred reactor (Correa, 1995). Here, the interaction of reaction and mixing is observed as a function of an imposed mixing frequency.

A more realistic test of scalar mixing models was performed by Nooren et al. (1997). For a natural gas–air diffusion flame, predicted temperature PDF's were compared to measured data for IEM, C/D and MCM mixing models. Although this case is representative for many jet diffusion flames, there is no direct comparison of the principal scalar variable (i.e. mixture fraction) with measured data.

In this study we directly compare mixture fraction, or equivalently the normalized jet fluid concentration, with predicted scalar mean, variance and PDF's. PDF predictions are governed by the mixing models only because we compare PDF's of the scaled concentration $C^* = C/\overline{C}$. This removes any dependence on the exact flow field predictions.

2.5. Flow configuration and numerics

The flow configurations studied are equal-density momentum-driven free turbulent jets (Dowling and Dimotakis, 1990). The specific jet flows are an ethylene (C_2H_4) jet in a nitrogen (N_2) reservoir at $\mathrm{Re} = 5000$ and a propylene (C_3H_6) jet in an argon (Ar) reservoir at Reynolds numbers 16000 and 40000. Several relevant flow properties like jet-reservoir density ratios, Schmidt numbers, inlet diameters and jet exit velocities are given in Table 1. The reservoir consists of a uniform low-velocity coflow with a velocity less than 0.006 of the jet exit velocity. The Reynolds number Re of the jet is based on the exit velocity U_0, the nozzle exit diameter d and the reservoir viscosity ν_∞. Measured jet exit turbulence levels are less than 0.2%.

It was found that the concentration field statistics obey a general self-similar scaling along rays emerging from the jets

Table 1
Relevant gas-mixture and flow properties (Dowling and Dimotakis, 1990)

	Re = 5000	Re = 16000	Re = 40000
Jet-reservoir density ratio	1.0015	1.053	1.053
Schmidt number	1.0	1.2	1.2
Inlet diameter d (mm)	19	7.62	7.62
Momentum diameter d^*	0.96 d	1.005 d	1.01 d
Jet exit velocity U_0 (m/s)	4.14	29.6	74.0

virtual origin (see Dowling and Dimotakis, 1990 and references therein). The term *general* similarity refers to similarity independent of Reynolds and Schmidt numbers. This in contrast to *specific* similarity which holds only for one specific Reynolds number and one specific Schmidt number. The general similarity for the mean concentration $\overline{C}$ takes the following form:

$$\overline{C}(x,r) = \kappa \frac{C_0 d^*}{x - x_0} g\left(\frac{r}{x - x_0}\right) = \kappa \frac{C_0}{\chi} g(\eta)$$

with C_0 the jet exit concentration, x_0 the location of the virtual jet origin and κ a scaling parameter. The scaled axial coordinate is given by $\chi = (x - x_0)/d^*$ and the similarity variable reads $\eta = r/(x - x_0)$. The self-similar radial profile is given by the function $g(\eta)$ with $g(0) = 1$. The configuration and the self-similar coordinate system are depicted in Fig. 1. Experimental PDF data is available at rays $\eta = 0, 0.06$ and 0.12, at different axial locations.

Because only far-field properties of the jet are studied, the exact inlet profiles are not important here. The jet inlet is modeled with uniform profiles for velocity, turbulent kinetic energy and dissipation. FVM calculations were subsequently performed at stretched rectilinear grids of 75×50, 150×100 and 110×75, and gird independent solutions are obtained at a grid of 110×75 cells for all three jets. Standard k–ϵ turbulence model with standard values for the constants is used.

Monte Carlo calculations are performed on a 110×75 grid for $\mathrm{Re} = 5000, 16\,000$ and $40\,000$. In the experiment the jet is unconfined but in the simulations a confinement is present to prevent numerical problems with outflow of Monte Carlo particles. The wall is located far from the axis such that it does not influence the flow in the jet region. To obtain sufficient statistical accuracy an ensemble of at least 100 particles per cell is used. Average concentration fields are obtained over 500–1000 iterations. To obtain accurate PDF estimates, a high number of statistically independent samples is required. From a stationary solution, particles are sampled every five iterations over a total of 6000–10 000 iterations. To obtain a large number of samples within a reasonable amount of time, some of the simulations are performed on a massively parallel CRAY-T3E using eight processors and approximately 50 particles per cell per processor.

Still the PDF's obtained in the far field (at $x/d \approx 90$), may suffer from a lack of statistically independent samples. This problem becomes clear by a simple example: At $x/d = 90$, $\Delta x/\overline{U} \approx 500\,\Delta t$, where Δx is the cell size, $\overline{U}$ the average axial velocity and Δt the time step of the simulation. This means that

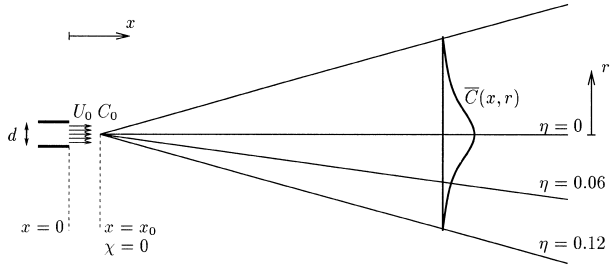

Fig. 1. Jet configuration with coordinate system (not to scale!). Physical coordinates: x, r, scaled axial coordinate: $\chi = (x - x_0)/d$, self-similar coordinate: $\eta = r/(x - x_0)$.

particles remain in the same cell for about 500 iterations. Furthermore, $1/\omega_\phi \approx 2000\,\Delta t$ which means that almost no mixing takes place here. As a result, the same particle scalar value is sampled $500/5 = 100$ times which effectively decreases the size of the ensemble by a factor 100.

3. Results

In this section, results of the Monte Carlo PDF method are compared to experimental data and FVM results. In the first part, self-similar scaling of concentration mean and variances is considered. This provides valuable information for the comparison of PDF shapes. In the second part, PDF shapes are compared. The performance of the mixing models and the importance of the micro-mixing in general are assessed.

3.1. Self-similar scaling of the concentration field

The measured mean concentration was found to be self-similar along rays emerging from the jets virtual origin. The scaling parameters κ and x_0 are determined by a least-squares estimate from the centerline profile of the mean concentration. Predicted fields do, in general, not scale with the same parameters as the experimental data. For $\mathrm{Re} = 5000$ this is illustrated in Fig. 2. Note that the estimated value of $\kappa = 7.25$ at $\mathrm{Re} = 40\,000$ deviates from the values obtained at lower Reynolds numbers ($\kappa = 5.8$). For the measured data, this parameter was estimated between 5.1 and 5.2. The scaling parameters x_0 and κ are summarized in Table 2.

Monte Carlo PDF sampling positions are calculated from the FVM estimate of x_0. Monte Carlo mean fields obey the

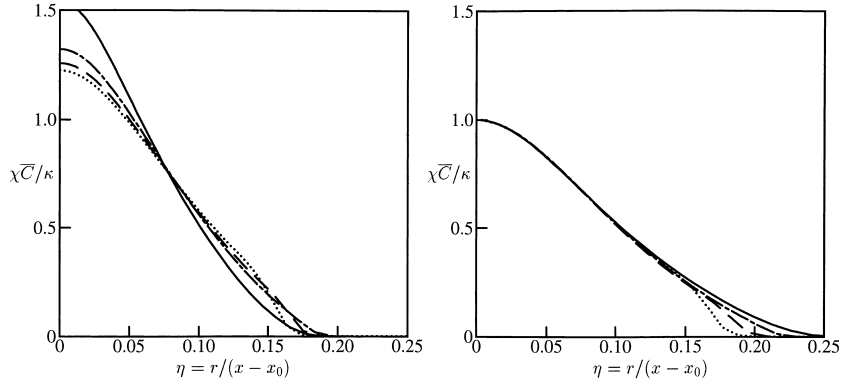

Fig. 2. Comparison of scaled mean concentration $\chi\bar{C}/\kappa$ for $\mathrm{Re} = 5000$ versus the scaled radial coordinate $\eta = r/(x - x_0)$. Left: scaling parameters estimated from experimental data, Right: scaling parameters estimated from FVM results. Lines: – – $x/d = 20$, – - – $x/d = 40$, - - - $x/d = 60, \ldots$ $x/d = 80$.

Table 2
Scaling parameters estimated from the centerline FVM mean concentration profiles. Reported parameters estimated from experimental data are given in brackets

Re	x_0/d		κ	
5000	2.65	(-3.7)	5.85	(5.11 ± 0.05)
16 000	2.38	(0.5)	5.83	(4.73 ± 0.1)
40 000	0.19	(0.5)	7.25	(between 5.1 and 5.2)

same scaling law but estimated values of the scaling parameters differ from FVM values. However, differences in PDF positions do not significantly influence the results.

The measured PDF's of C^* obey the general scaling for all three Reynolds numbers. A necessary condition for self-similarity of the PDF's is the fact that scalar RMS and the scalar mean follow the same scaling law. It was found that $C'_{\rm rms}/\overline{C}$ is constant along rays of constant η and that the ratio has a value of 0.23 ± 0.01 at the centerline. The FVM results show the same scaling behavior. The Monte Carlo results show the same constant ratio for $\chi > 30$ but the initial scalar decay and production of scalar variance are higher which results in a higher RMS-to-mean ratio at axial positions $\chi \approx 10$. As a result, PDF's at $\chi = 20, 30$ do not obey the self-similar scaling law. The overall behavior of $C'_{\rm rms}/\overline{C}$ for the Monte Carlo and FVM results is shown in Fig. 3. Statistical fluctuations in scalar mean *and* RMS cause large fluctuations in the Monte Carlo profiles even when fields are averaged over as many as 10 000 iterations. At Re = 40 000 (see Fig. 3), Monte Carlo predictions show a high RMS-to-mean ratio which increases to ≈ 0.33 at $\chi = 80$. As a result, PDF's at different axial positions have similar shape but with different variances.

3.2. Self-similar scaling of predicted PDF's

Fig. 4 depicts scalar PDF's at Re = 5000 for $\eta = 0$ and 0.06. Results of the C/D mixing model are compared to assumed-shape β-function PDF's. Assumed-shape PDF's are constructed using $C'_{\rm rms}/\overline{C} = 0.23$ and 0.34 at $\eta = 0$ and 0.06 respectively. At the centerline, the similarity of the PDF's at $x/d = 40, 60$ and 80 and the β-function is very good. At $x/d = 20$, the Monte Carlo model predicts the correct PDF shape but overpredicts the variance which was already indicated by the high RMS-to-mean ratio (see Fig. 3). At 3.4° off centerline ($\eta = 0.06$), the similarity of the C/D predictions is good but, in comparison with the assumed-shape PDF, the peak at $C^* = 1$ is too narrow and the tail at high C^* is overpredicted. IEM, MCM and BL models predict PDF shapes that are more skewed towards low concentrations. For these models, differences in the PDF's obtained at different axial locations are larger than for the C/D predictions.

At Re = 16 000, Monte Carlo PDF shapes are the same as those observed at Re = 5000. However, fluctuations in the RMS-to-mean ratio cause that variances are too large for some PDF's (for different models and at different axial locations). In general however, along rays of constant η, PDF's scale more accurately at Re = 16 000 than at Re = 5000.

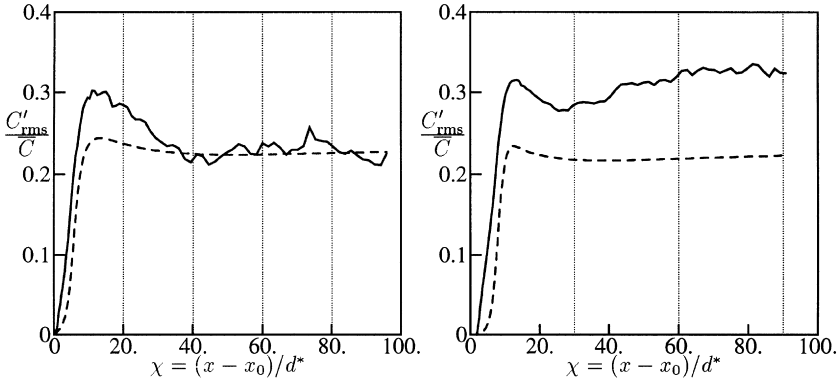

Fig. 3. Centerline scalar RMS-to-mean ratio versus scaled axial coordinate. Left: Re = 5000. Right: Re = 40 000. Results at Re = 16 000 are similar to those at Re = 5000. Lines: – – – Monte Carlo with C/D model, – – – FVM, Vertical lines represent axial locations of sampled PDF's.

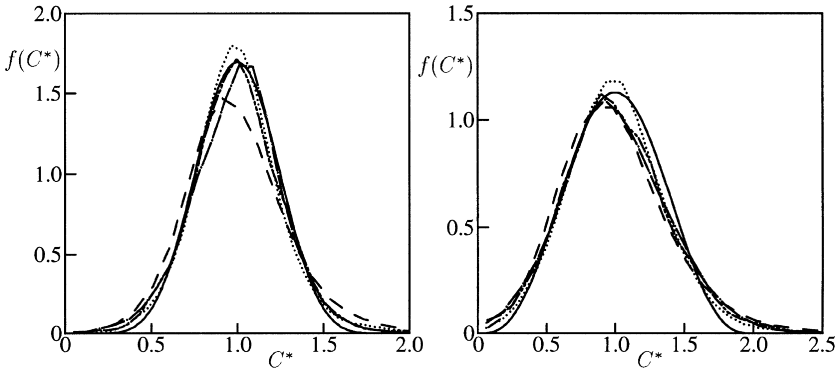

Fig. 4. Predicted scalar PDF $f(C^*)$ for Re = 5000. Left: $\eta = 0$ Right: $\eta = 0.06$. Lines: – – – assumed-shape β-function; Monte Carlo with C/D model: – – – $x/d = 20$, ... $x/d = 40$, –·– $x/d = 60$, – - - – $x/d = 80$.

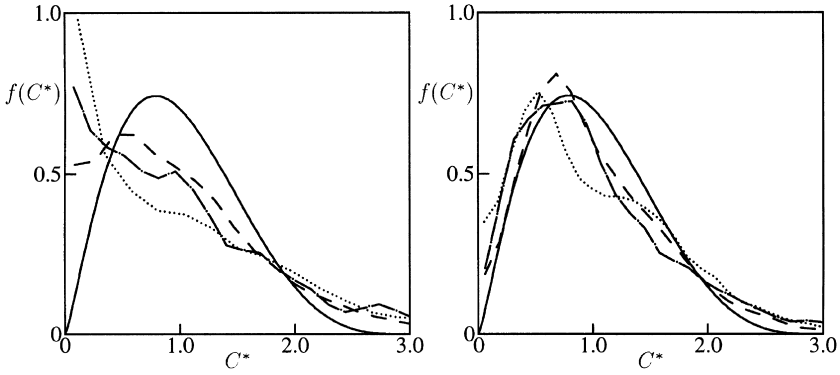

Fig. 5. Predicted scalar PDF's at $\eta = 0.12$ for Re = 16000. Left: C/D model Right: BL model Lines: – – assumed-shape β-function; Monte Carlo predictions at: – – – $x/d = 30, \ldots$ $x/d = 60$, –·– $x/d = 90$.

At 7° off centerline ($\eta = 0.12$), the general picture is quite different from that observed at $\eta = 0$ and 0.06. In Fig. 5, the PDF's predicted by C/D and BL models are depicted for Re = 16000. The behavior at Re = 40000 is the same. Here, the C/D model predicts a high probability at low concentrations and the PDF is peaked at $C^* = 0$, at large axial distances. The PDF's predicted by IEM, BL and MCM models are zero for $C^* = 0$. Remarkably, BL results are very good in comparison with the other Monte Carlo results. Note that the assumed-shape β-function PDF is zero for $C^* = 0$ by construction. The behavior of the C/D model is consistent with that observed in pure mixing in homogeneous isotropic turbulence (see Section 2.4). There, the C/D model overpredicts the tails of the PDF. In the far field, away from the centerline, the mixing frequency is low and the probability of finding unmixed particles with zero concentration at the edge of the jet is not zero, using the C/D model.

As shown in the previous section, the Monte Carlo RMS-to-mean ratio is not constant at Re = 40000 and predicted PDF's have the same shape but do not scale correctly. In the following, the Re = 40000 only, scalar fluctuations are rescaled such that the RMS-to-mean ratio equals that of the measurements.

3.3. Comparison with measured PDF's

In this section, Monte Carlo PDF's are compared to measured data. Because assumed-shape β-function PDF's agree well with the measurements for all Reynolds numbers, for all axial and radial positions, results of the FVM are not shown here.

In Fig. 6, the centerline PDF's are shown for Re = 5000 and 16000. Measured PDF's are estimated from the data published by Dowling and Dimotakis (1990). Error bars indicate the observed unsystematic differences in the PDF's at different axial positions. Presented Monte Carlo PDF's are averages of the PDF's at $x/d = 40, 60$ and 80 for Re = 5000, and at $x/d = 30$, 60 and 90 for Re = 16000. For Re = 40000, PDF variances are rescaled before PDF's are averaged over the axial locations. Measured PDF's at Re = 40000 resemble those obtained at Re = 5000. At Re = 40000, measurements were performed at $x/d = 60$ only and no error bars can be estimated from the published data. For this reason, predicted PDF's at Re = 40000 are compared with the measurements obtained at Re = 5000.

At the centerline, the C/D model predictions are perfect for Re = 5000 and 40000 and predictions are good for Re = 16000. The PDF is within the observed range for almost all values of C^*. PDF's predicted by IEM, BL and MCM models are skewed towards small concentrations and the maximum is located at $C^* \approx 0.94$ compared to $C^* = 1$ for the measured data and the C/D predictions. The overprediction of the tails at high C^* is caused by a high RMS-to-mean ratio. The underprediction of the maximum for IEM, MCM and BL models remains after rescaling of the PDF variances.

Fig. 7 depicts the PDF's at $\eta = 0.06$ for Re = 16000 and 40000. The fact that, at certain values of η, the Monte Carlo model yields a too high and non-constant RMS-to-mean ratio

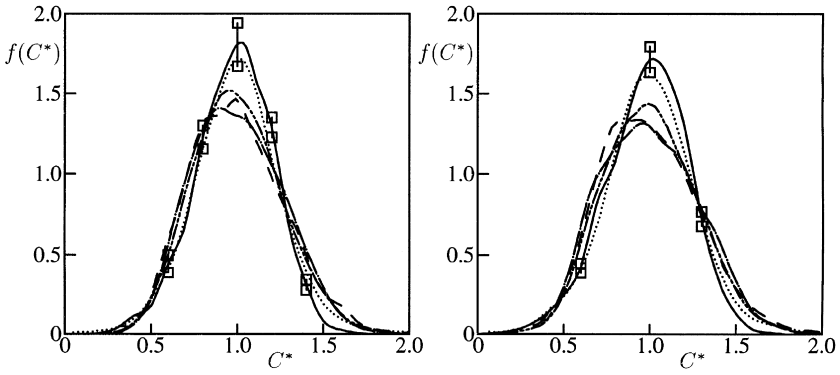

Fig. 6. Centerline scalar PDF's for: Left: Re = 5000 and Right Re = 16000. Lines: – – measurement, □ error bars; Monte Carlo predictions: – – – IEM, … C/D, –·– MCM, – - - – BL.

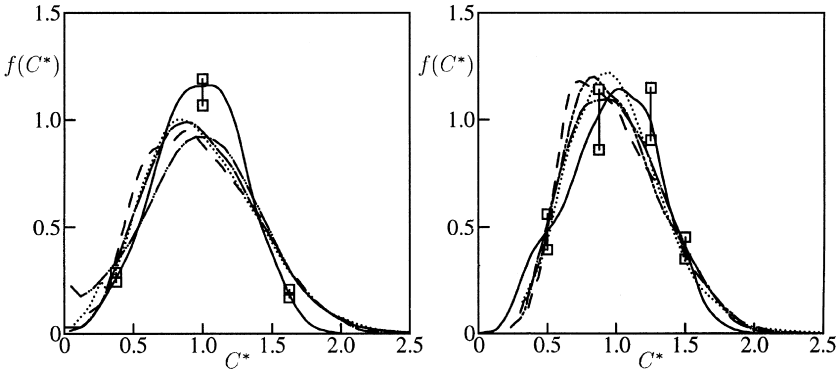

Fig. 7. Scalar PDF's at 3.4° off centerline for: Left: Re = 16000 and Right: Re = 40000, here the measurements are those at Re = 5000 (error bars are likely to be larger for Re = 40000). Lines are the same as those of Fig. 6.

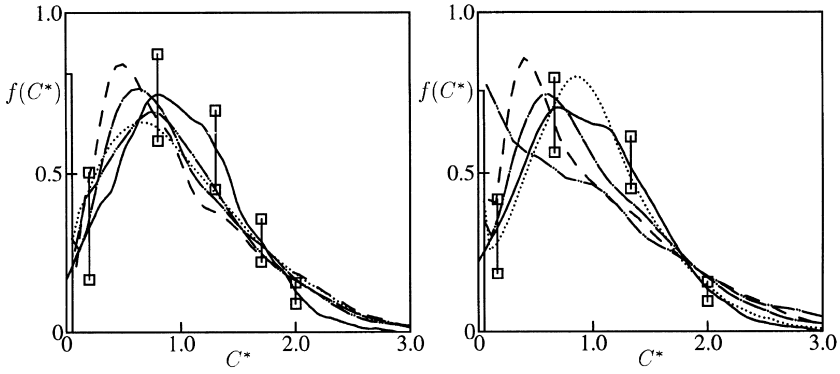

Fig. 8. Scalar PDF's at 7° off centerline for: Left: Re = 5000 and Right: Re = 16000. Lines are the same as those of Fig. 6. The peak at $C^* = 0$ indicates the maximal intermittency observed.

is clearly seen in Fig. 7. Predicted PDF shapes are correct but the variance is overestimated severely. For Re = 40000, predictions agree well with the experimental data but no distinct differences between model predictions are observed. The averaged predicted PDF's at Re = 5000, show the same features that were observed for Re = 16000.

PDF's at 7° off centerline, for Re = 5000 and 16000, are depicted in Fig. 8. The measured peak at $C^* = 0$ indicates the observed maximal intermittency. This represents the probability that unmixed reservoir fluid is measured in the jet region. The scatter in the measured PDF's around $C^* = 0$ is very large which is caused also by the intermittent character of the jet at rays far from the centerline. Because of the large scatter in the experimental data, all model predictions fall within the observed range for most C^* values. Again, the IEM model predicts a peak around $C^* = 0.5$ compared to a higher most likely value of $C^* \approx 0.8$ for the measured data. MCM and BL perform better at these positions than at rays closer to the centerline. The C/D model, which performs well close to the centerline, fails to predict the correct PDF shape at the edge of the jet. At Re = 5000 results are reasonable but at higher Reynolds numbers, the PDF increases almost linearly for $C^* \to 0$. This behavior is caused by the stochastic pairwise mixing process which was mentioned in the previous section. This result is not caused by intermittency effects like those observed in the experiment. The present PDF model assumes one mean turbulent frequency and it does not mimic effects of intermittency. IEM, MCM and BL models contain a deterministic drift term to the mean and correctly predict a decreasing probability for $C^* \to 0$.

4. Conclusions

Accurate prediction of mixture fraction PDF's with the Monte Carlo PDF method requires highly CPU-intensive simulations performing many iterations with a sufficiently high number of particles per cell. Further computations, thereby increasing the number of statistically independent samples did not directly improve the PDF's presented here. Still, in the far field, PDF's may suffer from an insufficient number of statistically independent samples. A detailed comparison of PDF's of the normalized concentration $C/\overline{C}$ is difficult because of large statistical fluctuations in the predicted RMS-to-mean ratio.

Close to the centerline, PDF predictions are reasonable for all models. The IEM model always underpredicts the most likely concentration value. MCM and BL models show this defect near the centerline but results improve at larger radial distances. At 7° off centerline, BL PDF predictions agree very well with the measured data.

The C/D model performs very well at positions close to the jet centerline. The most likely concentration value is predicted correctly and the PDF shape agrees well with the measurements. At the edge of the jet, where the experimental data show the effects of intermittency, the C/D model predicts an almost linearly increasing PDF with decreasing concentration. The PDF model does not account for effects of intermittency and the 'linear' PDF shape is caused by the nature of the stochastic pairwise mixing process of the C/D model.

Remarkably, the FVM assumed-shape β-function PDF agrees very well with the experimental data for all positions.

The FVM yields the correct RMS-to-mean ratio. Apparently, the a-priori assumption of a β-function PDF which is parametrized by scalar mean and variance, works well in single-conserved-scalar methods. Effects of intermittency are not captured by our FVM model.

This study has shown details of the effects of micro-mixing on the predicted scalar PDF's. Different mixing models show no distinct differences in scalar PDF shapes. Apparently, turbulent convection is the dominant force in scalar mixing in these inhomogeneous jet flows. Mixing model performance in jet diffusion flame simulations will depend on the value of the stoichiometric mixture fraction and the location of the stoichiometric contour with respect to the edge of the jet. Further insight in the effects of micro-mixing in turbulent reacting jet flows may be gained by combining the results of this study with similar studies of jet diffusion flames.

Appendix A. Modified BL model

In the BL model, the effects of micro-mixing are modeled by a relaxation of all scalar particles to the local mean combined with a random diffusion term that models the effects of turbulent dispersion. In terms of a stochastic model for scalar particles ϕ^* the model reads

$$\mathrm{d}\phi^* = A(\phi^* - \overline{\phi})\,\mathrm{d}t + B^{1/2}\,\mathrm{d}W.$$

Here $\mathrm{d}W$ is a stochastic Wiener increment and A and B are respectively the drift and diffusion coefficients which read

$$A = -\frac{1}{2}\omega_\phi\left[1 + \kappa\left(1 - \frac{\overline{\psi'^2}}{\psi^2}\right)\right],$$

$$B = \left[\kappa\left(1 - \frac{(\phi^* - \overline{\phi})^2}{\psi^2}\right)\overline{\phi'^2}\omega_\phi\right]$$

in which ω_ϕ is the scalar variance decay rate and κ a model parameter that takes here the value 0.6. The diffusion coefficient B is constructed such that it goes to zero at the physical bounds of the scalar (i.e. $\phi_{\min}$ and $\phi_{\max}$). The model terms ψ^2 and $\overline{\psi'^2}$ are defined as:

$$\psi^2 = (\phi_{\max} - \overline{\phi})^2 \quad \text{and} \quad \overline{\psi'^2} = \langle \phi'^2 | \phi' > 0 \rangle \ \text{ for } \phi^* > \overline{\phi},$$

$$\psi^2 = (\phi_{\min} - \overline{\phi})^2 \quad \text{and} \quad \overline{\psi'^2} = \langle \phi'^2 | \phi' < 0 \rangle \ \text{ for } \phi^* < \overline{\phi}.$$

This modification of the standard model by Valiño and Dopazo (1991) is made to handle the mixing of asymmetric scalar PDF's correctly.

References

Chen, H., Chen, S., Kraichnan, R.H., 1989. Probability distribution of a stochastically advected scalar field. Physical Review Letters 63 (24), 2657–2660.

Correa, S.M., Pope, S.B., 1992. Comparison of a Monte Carlo PDF/finite-volume mean flow model with bluff-body Raman data. 24th International Symposium on Combustion, pp. 279–285.

Correa, S.M., 1995. A direct comparison of pair-exchange and IEM models in premixed combustion. Combustion and Flame 103 (3), 194–206.

Curl, R.L., 1963. Dispersed phase mixing: I. Theory and effects in simple reactors. Journal of the American Institute of Chemical Engineers 9 (2), 175–181.

Dopazo, C., 1975. Probability density function approach for a turbulent axisymmetric heated jet. Centerline evolution. The Physics of Fluids 18, 397–404.

Dowling, D.R., Dimotakis, P.E., 1990. Similarity of the concentration field of gas-phase turbulent jets. Journal of Fluid Mechanics 218, 109–141.

Eswaran, V., Pope, S.B., 1988. Direct numerical simulations of the turbulent mixing of a passive scalar. The Physics of Fluids 31 (3), 506–520.

Haworth, D.C., El Tahry, S.H., 1990. Probability density function approach for multidimensional turbulent flow calculations with application to in-cylinder flows in reciprocating engines. AIAA Journal 29 (2), 208–218.

Haworth, D.C., Pope, S.B., 1986. A generalized Langevin model for turbulent flows. The Physics of Fluids 29, 387–405.

Janicka, J., Kolbe, W., Kollmann, W., 1979. Closure of the transport equation for the probability density function of turbulent scalar fields. Journal Non-Equilibrium Thermodynamics 4, 47–66.

Nooren, P.A., Wouters, H.A., Peeters, T.W.J., Roekaerts, D., Maas, U., Schmidt, D., 1997. Monte Carlo PDF modelling of a turbulent natural-gas diffusion flame. Combustion Theory and Modelling 1 (1), 79–96.

Pope, S.B., 1985. PDF methods for turbulent reactive flows. Progress in Energy and Combustion Science 11, 119–192.

Pope, S.B., 1990. Computations of turbulent combustion: progress and challenges. 23rd International Symposium on Combustion, pp. 591–612.

Pope, S.B., 1991. Mapping closures for turbulent mixing and reaction. Theoretical Comput. Fluid Dynamics 2, 255–270.

Valiño, L., Dopazo, C., 1991. A binomial Langevin model for turbulent mixing. Physics of Fluids A 3 (12), 3034–3037.

Warhaft, Z., Lumley, J.L., 1978. An experimental study of the decay of temperature fluctuations in grid-generated turbulence. Journal of Fluid Mechanics 88, 659–684.